FRONTIERS OF PHYSICS

RESEARCH ARTICLE
Volume 19 / Issue 5 / 54202 / 2024

# Holographic images of an AdS black hole within the framework of $f(R)$ gravity theory

Guo-Ping Li[1,†], Ke-Jian He[2], Xin-Yun Hu[3], Qing-Quan Jiang[1,‡]

1 School of Physics and Astronomy, China West Normal University, Nanchong 637000, China
2 College Of Physics, Chongqing University, Chongqing 401331, China
3 College of Economic and Management, Chongqing Jiaotong University, Chongqing 400074, China
Corresponding authors. E-mail: †gpliphys@yeah.net, ‡qqjiangphys@yeah.net
Received November 2, 2023; accepted February 19, 2024



**ABSTRACT**

Based on the AdS/CFT correspondence, this study employs an oscillating Gaussian source to numerically study the holographic images of an AdS black hole under $f(R)$ gravity using wave optics. Due to the diffraction of scalar wave, it turns out that one can clearly observed the interference patten of the absolute amplitude of response function on the AdS boundary. Furthermore, it is observed that its peak increases with the $f(R)$ parameter $\alpha$ but decreases with the global monopole $\eta$, frequency $\omega$, and horizon $r_h$. More importantly, the results reveal that the holographic Einstein ring is a series of concentric striped patterns for an observer at the North Pole and that their center is analogous to a Poisson–Arago spot. This ring can evolve into a luminosity-deformed ring or two light spots when the observer is at a different position. According to geometrical optics, it is true that the size of the brightest holographic ring is approximately equal to that of the photon sphere, and the two light spots correspond to clockwise and anticlockwise light rays. In addition, holographic images for different values of black holes and optical system parameters were obtained, and different features emerged. Finally, we conclude that the holographic rings of the AdS black hole in modified gravities are more suitable and helpful for testing the existence of a gravity dual for a given material.

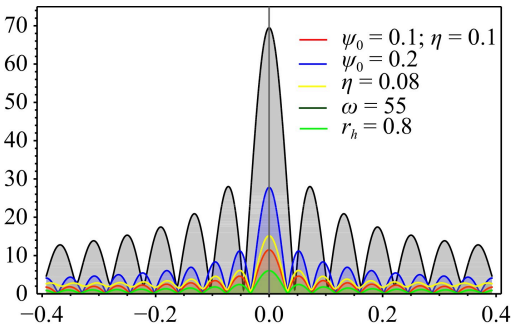


**Keywords** AdS black hole, holographic images, AdS/CFT correspondence

## 1 Introduction

The holographic principle was proposed as a fundamental property of relativistic gravity, which is primarily based on the thermodynamics of black holes [1, 2]. As a concrete realization of the holographic principle, the AdS/CFT correspondence states that the quantum gravity theory in a $(d+1)$-dimensional anti-de Sitter ($AdS_{d+1}$) space-time is equivalent to the d-dimensional conformal quantum field theory ($CFT_d$) on the boundary [3]. A precise mathematical relationship for this correspondence can be established by computing various physical quantities on both sides [3–5]. AdS/CFT duality has two important characteristics: the duality between gravitational theory and lower-dimensional non-gravitational theory, which reflects the holographic principle, and the duality between weak coupling gravitational theory and strong coupling field theory. These characteristics allow for the exploration of the quantum nature of gravity using field

https://doi.org/10.1007/s11467-024-1393-8

theory and the study of field theory using the gravity dual. For example, holographic gauge theory models have been used to compute experimentally measured observables in quantum chromodynamics (QCD) [6]. Holographic condensed-matter models exhibit the characteristic behavior of superconductors, providing a novel method for studying strongly coupled condensed-matter systems [7]. New insights into the hydrodynamics of fluids have been obtained from the computation of perturbations near a black-hole horizon [8–10]. The AdS/CFT correspondence, or more generally the gauge/gravity duality, gauge/string duality, has been extended to general cases without supersymmetry or conformal symmetry [11–15]. It continues to inspire many studies in various fields of physics [16–22]. For example, the holographic prescription has recently been regarded as a useful tool for studying aspects of quantum information in gravity and field theories, including mutual information [16, 17], entanglement entropy [18], and computational complexity [19]. In cosmology, several holographic models have been proposed to explain the nature of dark energy [20–22]. Other holographic correspondence models have been discussed, such as the dS/CFT and Kerr/CFT correspondences [23, 24]. Therefore, the AdS/CFT duality has been proven to be a powerful tool for studying physical processes that occur in a gravitational background or have a gravity dual [25–40].

The discovery of the gravitational wave (GW150914) by the Laser Interferometer Gravitational Wave Observatory (LIGO) dispelled any doubts regarding the existence of black holes in the Universe. [41]. More importantly, the Event Horizon Telescope (EHT) collaboration captured shadows of supermassive black holes in the center of the giant elliptical galaxy $M87^*$ and the Milky Way [42, 43]. Based on these observations, each shadow comprises a dark central region surrounded by a bright ring. Theoretically, the dark region is generally called a black-hole shadow, whereas the bright ring is a photon ring. This demonstrates that the observational appearance of black holes with the inclusion of shadows and rings can give rise to a thoughtful understanding of the fundamental properties of black holes. An increasing number of studies have been conducted recently on this topic Refs. [44–64]. For instance, the size and shape of shadows for different black hole parameters were carefully addressed in Refs. [44–51]. When black holes are surrounded by different classes of luminous accretion, observational shadows, and rings are described in different gravity theories [53–64]. On the other hand, it is well known that if a light source behind it illuminates a gravitational body, the observer on the other side of the same line will also capture a ring-like image owing to gravitational lensing. This ring-like image is called an Einstein ring in astronomy and has attracted considerable attention [65–72]. Black holes possess strong gravity. Light rays may surround black holes several times, allowing multiple Einstein rings to emerge naturally. Therefore, as the observational appearance of the black hole shadow, the Einstein ring can shed light on the fundamental properties of black holes because general relativity theory implies that the Einstein ring is equivalent to a photon ring. Recently, based on the AdS/CFT correspondence, the holographic Einstein ring of the AdS black hole in the bulk from a given response function on the boundary was constructed for the first time using a direct procedure [73, 74]. This simple method provides a useful tool for determining whether dual gravity exists for given quantum field theories (QFTs). In 2021, employing this method, researchers observed the holographic image of an asymptotic AdS black hole dual to a superconductor on a two-dimensional sphere [75], further affirming the existence of black holes through tabletop experiments with superconductors as long as they have gravitational duals. Subsequently, this idea was generalized to other anti-de Sitter black holes using more precise numerical techniques [76–81]. These studied reveal that the possible generalizations and applications of holographic images of AdS black holes are very important, as they can be regarded as an experimental test for the existence of a gravitational dual of a given material.

Einstein gravity, namely, general relativity (GR), for which the holographic rings of the AdS black hole have recently been detailed [73, 74, 76], is regarded as a successful theory only for describing the gravitational interaction between submillimeter and solar system scales [82]. However, Planck's length is generally expected to be replaced by the quantum theory of gravity with ultraviolet completion [83]. Owing to the absence of fundamental quantum gravity, modified gravity, as a phenomenological model representing a classical generalization of the GR, was constructed by complying with observational data and data from local tests. Therefore, it is evident that the holographic rings of AdS black holes in modified gravities would be more suitable than Einstein gravity. However, the features of holographic Einstein images in modified gravities remain unknown in the holographic framework. Therefore, this study aims to address this gap in the literature. It is well-known that Einstein's field equation can be obtained using the least-action principle. The Lagrangian function of the action is the Ricci scalar $R$. However, Einstein's field equation must be modified to study the Universe's accelerated expansion. Therefore, it is natural to correct the Lagrangian function of the action as a function of $R$, that is, $f(R)$, rather than $R$ itself. Buchdahl realized this idea in 1970 and proposed the well-known $f(R)$ theory. Therefore, $f(R)$-gravity theory, as a type of modified gravity theory, has been regarded as a good candidate for explaining the accelerating Universe. This is attributed to its capacity to account for the accelerating phases during the early and late epochs of the universe [84–87]. Accordingly, considerable effort has been devoted to studying various aspects of this gravity

theory and a series of results have been obtained [88–97]. For instance, one study not only found various black holes using $f(R)$ theory but also further investigated the effects of corresponding parameters on their thermodynamic properties [88–90]. In the $f(R)$ theory context, strong gravitational lensing, thermodynamic phase transitions, and gravitational wave propagation have been carefully discussed [92–94]. In addition, the shadows and rings of black holes surrounded by various accretions were obtained, and a few useful constraints on $f(R)$ parameter were discussed [58]. For more detailed aspects of $f(R)$ theory, please refer to Refs. [98, 99]. Building upon the abovementioned results, we consider $f(R)$ gravity as an example of a modified gravity to present the preferable holographic images of a dual black hole, assuming a dual gravitational picture exists for a given quantum system. In particular, based on the AdS/CFT correspondence, we employed an oscillating Gaussian source to numerically study the holographic images of an AdS black hole using wave optics and then further clarified the corresponding results using geometrical optics.

The remainder of this paper is organized as follows: Section 2 is devoted to introducing the construction of the holographic image. In Section 3, by considering the oscillating Gaussian source on the AdS boundary, we carefully study the scalar field and response function of the AdS black hole in massive gravity. In Section 4, we present the holographic images of a $f(R)$ AdS black hole with the aid of a lens and screen and further analyze these images using geometrical optics. Finally, Section 5 presents our conclusions and a discussion.

## 2 Construction of the holographic image

A schematic of the imaging of a dual black hole is shown in Fig. 1. On the AdS boundary, we consider a scalar wave generated by the source $\mathcal{J}_O$ at a certain point that

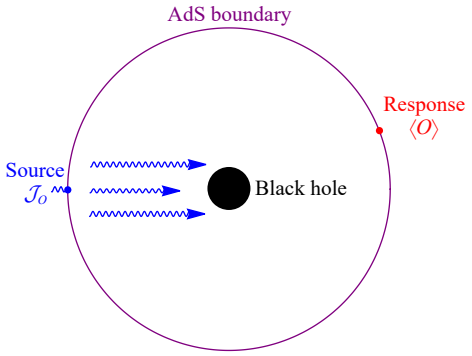


**Fig. 1** Schematic of the imaging of a dual black hole.

will be injected into the bulk because of the time-periodic boundary condition. From this point, the wave propagates in the AdS space-time and reaches another point on the AdS boundary. The arriving boundary scalar wave is identified as the response function $\langle O\rangle$. $\langle O\rangle$ contains the characteristic information of an AdS black hole. In general, source $\mathcal{J}_O$ can be fixed to an oscillating Gaussian source as the boundary condition for the scalar field. In this case, one can see that the (2+1)-dimensional boundary CFT on the 2-sphere $S^2$ is dual to a black hole in the global $AdS_4$ space-time or a massless bulk scalar field in this space-time.

If the response function $\langle O\rangle$ can be successfully obtained, the detailed transformation can be expressed as shown in Fig. 2.

For arbitrary positions of the source and response functions, we can always choose an appropriate coordinate system to ensure preferred observation positions $(\theta_{obs}, 0)$, where position $\mathcal{J}_O$ is located at the South Pole, as shown in Fig. 2(a). To convert the response function to a black hole image, we still require an optical system with the inclusion of two proper components at the boundary, a convex lens and a spherical screen. A lens with focal length $f$ and radius $d$ converts a plane wave ($pw$) into a

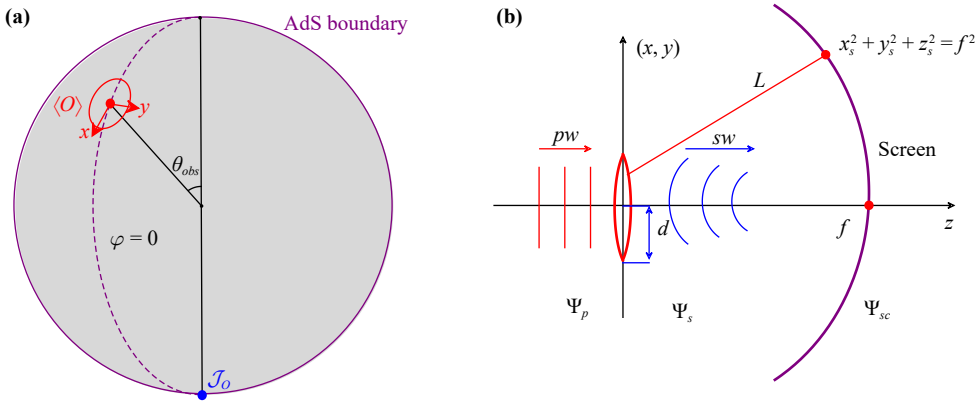


Position of $\mathcal{J}_O$ and $\langle O\rangle$ .

Forming the transmitted wave on the screen

**Fig. 2** Detailed transformation of the response function $\langle O\rangle$ on the screen.

spherical wave ($sw$) and the spherical screen presents an image of a dual black hole, as shown in Fig. 2(b). Here, the convex lens is fixed to the coordinates $\boldsymbol{x} = (x, y, 0)$ of the flat 3-dimensional space $(x, y, z)$, and the coordinates of the observed point on the screen are defined as $(\boldsymbol{x}_S = x_S, y_S, z_S)$. In the optical system [Fig. 2(b)], the response function near the observation positions is first copied as $\Psi_p$. Then, when the observer looks up into the AdS bulk using this system, the function $\Psi_{sc}$ is obtained to construct an image of a dual black hole.

## 3 Scaler field and response function of the AdS black hole in $f(R)$ gravity

This section introduces the AdS black hole solution under $f(R)$ gravity. Recently, a class of exact solutions for modified field equations with a global monopole was obtained that generalized previous results in the $f(R)$ theory of gravity [100]. Considering a negative cosmological constant, the corresponding action of $f(R)$ gravity is

$$\mathcal{S} = \frac{1}{16\pi}\int \mathrm{d}^4x\sqrt{-g}\left[f(R) + \mathcal{L}\right], \tag{1}$$

where $g$ is the determinant of a $4\times 4$ matrix, $\mathcal{L}$ represents the Lagrangian density, and the natural unit $G \equiv c \equiv \hbar \equiv 1$ is adopted throughout the study. This action generates the following field equations:

$$\begin{aligned}\kappa T_{\mu\nu} = {} & F(R)R_{\mu\nu} - \frac{1}{2}f(R)g_{\mu\nu} - \nabla_\mu\nabla_\nu[F(R)] \\ & + \Box[F(R)]g_{\mu\nu},\end{aligned} \tag{2}$$

where $F(R) = \mathrm{d}f(R)/\mathrm{d}R$, $\kappa = 8\pi$. The Lagrangian density, considering the global monopole space-time model, is described by

$$\mathcal{L} = \frac{1}{2}\partial_\mu\phi^\alpha\partial^\mu\phi^\alpha - \frac{1}{4}\lambda(\phi^\alpha\phi^\alpha - \eta^2)^2. \tag{3}$$

Here, $\lambda$ is the positive coupling constant that disappears in the energy-momentum tensor [101], and $\eta$ represents the spontaneous breaking of $O(3)$ symmetry to $U(1)$ symmetry. However, $\phi^\alpha$ is given by an isotriplet of scalar fields corresponding to the well-known hedgehog ansatz [101]. From the above equations, a static black hole solution is obtained as follows:

$$\mathrm{d}s^2 = -A(r)\mathrm{d}t^2 + \frac{1}{B(r)}\mathrm{d}r^2 + r^2\mathrm{d}\theta^2 + r^2\sin\theta^2\mathrm{d}\varphi^2, \tag{4}$$

with

$$A(r) = B(r) = 1 - 8\pi\eta^2 + 3M\psi_0 - \frac{2M}{r} - \psi_0 r + \frac{\tilde{\Lambda}}{3}r^2. \tag{5}$$

In Eq. (5), $\psi_0$ originates from $f(R)$ gravity, and $\psi_0 r$ represents the deviation from general relativity. We always define $F(R) = \mathrm{d}f(R)/\mathrm{d}R$ and $F(R) = 1$ according to Einstein's GR theory. Additionally, because $R$ is a function of $r$, we have $F(R) = F(R(r))$. Generally, the function $F(R(r))$ can be expressed as $F(R(r)) = 1 + \psi(r)$; for simplicity, we take $\psi(r)$ as $\psi(r) = \psi_0 r$ to study holographic images under $f(R)$ gravity. Therefore, one can see that the effect of $f(R)$ gravity is embodied in the parameter $\psi_0$. In addition, $M$ is related to the black hole mass, $\tilde{\Lambda} = 3/\ell^2$, where $\ell$ is the AdS radius and the cosmological constant $\tilde{\Lambda}$ originates from some parameters of the metric coefficient. By introducing a new coordinate $(t, u, \theta, \varphi)$ into the metric (4), it can be reexpressed as $f(u)$, where $u = 1/r$. Therefore, we further employ the Eddington ingoing coordinates as follows:

$$v = t + u_* = t - \int\frac{\mathrm{d}u}{f(u)}. \tag{6}$$

Therefore, the metric can be rewritten as

$$\mathrm{d}s^2 = \frac{1}{u^2}\left[-f(u)\mathrm{d}v^2 - 2\mathrm{d}u\mathrm{d}v + \mathrm{d}\theta^2 + \sin\theta^2\mathrm{d}\varphi^2\right], \tag{7}$$

where

$$\begin{aligned}f(u) = {} & 1 + \frac{1}{u^2} - \frac{\psi_0}{u} - 8\pi\eta^2 \\ & + \frac{3\psi_0\left[1 - \psi_0 u_h + \left(1 - 8\pi\eta^2\right)u_h^2\right]}{u_h^2\left(2u_h - 3\psi_0\right)} \\ & - \frac{2u\left[1 - \psi_0 u_h + \left(1 - 8\pi\eta^2\right)u_h^2\right]}{u_h^2\left(2u_h - 3\psi_0\right)},\end{aligned} \tag{8}$$

and where $u_h = 1/r_h$ and $r_h$ is the event horizon of the black hole, which is determined using the equation $A(r) = 0$. Considering a massless particle in a scalar field, its dynamics can be described by the Klein–Gordon equation,

$$\Box\Phi(v, u, \theta, \varphi) = 0, \tag{9}$$

in the proposed coordinate system. Its exact form is

$$\begin{aligned}& u^2 f(u)\partial_u\partial_u\Phi + \left[u^2 f'(u) - 2uf(u)\right]\partial_u\Phi - 2u^2\partial_v\partial_u\Phi \\ & \quad + 2u\partial_v\Phi + u^2 D_S^2\Phi = 0,\end{aligned} \tag{10}$$

where $f'(u) = \partial_u f(u)$ near the AdS boundary, that is, $u \to 0$. The asymptotic solution to the above equation is [76]

$$\begin{aligned}\Phi(v, u, \theta, \varphi) = {} & \mathcal{J}_O(v, \theta, \varphi) + u(\partial_v)\mathcal{J}_O(v, \theta, \varphi) \\ & + \frac{1}{2}u^2(D_S^2)\mathcal{J}_O(v, \theta, \varphi) + u^3\langle O\rangle + \mathcal{O}(u^4).\end{aligned} \tag{11}$$

$D_S^2$ is the scalar Laplacian of unit $S^2$. Based on the AdS/CFT dictionary, $\mathcal{J}_O$ and $\langle O\rangle$, as independent functions of the boundary coordinates $(v, \theta, \varphi)$, are the external scalar source and the corresponding response function in the

dual CFT, respectively. By choosing a monochromatic and axis-symmetric Gaussian wave packet source located at the south pole of the AdS boundary as the source, we obtain

$$\mathcal{J}_O(v,\theta) = \mathrm{e}^{\mathrm{i}\omega v}\cdot\frac{1}{2\pi\sigma^2}\cdot\exp\left[-\frac{(\pi-\theta)^2}{2\sigma^2}\right] = \mathrm{e}^{\mathrm{i}\omega v}\cdot\sum_{l=0}^{\infty}c_{l0}Y_{l0}(\theta), \tag{12}$$

with

$$c_{l0} = (-1)^l\sqrt{\frac{l+1/2}{2\pi}}\exp\left[-\frac{1}{2}(l+1/2)^2\sigma^2\right]. \tag{13}$$

In Eq. (12), $\sigma$ represents the width of the wave produced by the Gaussian source, and it should be noted that the case $\sigma \ll \pi$ is only considered because the small value of the Gaussian tail can be ignored. In addition, $Y_{l0}$ is a spherical harmonic function. Owing to the symmetry of the space-time and source (Eq. (12)), the scalar field $\Phi$ can be decomposed as

$$\Phi(v,u,\theta,\varphi) = \mathrm{e}^{\mathrm{i}\omega v}\cdot\sum_{l=0}^{\infty}c_{l0}U_l(u)Y_{l0}(\theta,\varphi). \tag{14}$$

Correspondingly, the response function is

$$\langle O\rangle = \mathrm{e}^{\mathrm{i}\omega v}\sum_l\langle O\rangle_l Y_{l0}(\theta). \tag{15}$$

By substituting Eq. (14) into Eq. (10), we obtain

$$u^2 f(u)U_l'' + \left[u^2 f'(u) - 2uf(u) + 2\mathrm{i}\omega u^2\right]U_l' - \left[2\mathrm{i}\omega u + l(l+1)u^2\right]U_l = 0. \tag{16}$$

Combining this with Eq. (14), Eq. (11) is

$$\lim_{u\to 0}U_l = 1 - (\mathrm{i}\omega)u + \frac{1}{2}\left[-l(l+1)\right]u^2 + \langle O\rangle_l u^3 + \mathcal{O}(u^4). \tag{17}$$

To determine the total response function $\langle O\rangle$, Eq. (16) is used to obtain $U_l$. Then, $\langle O\rangle_l$ can be extracted using Eq. (17). Finally, one can obtain the total response function $\langle O\rangle$ with the relationship (15). Here, we employ the pseudospectral method [76] to solve Eq. (16) by considering the boundary conditions at the horizon and AdS boundary. At the boundary, that is, $u=0$, we have $U_l(0)=1$. For the horizon, $u=u_h$, Eq. (16) can be expressed as $\left[u_h^2 f'(u_h)+\mathrm{i}2\omega u_h^2\right]U_l' - \left[2\mathrm{i}\omega u_h + l(l+1)u_h^2\right]U_l = 0$. By choosing $\sigma = 0.05$ and $d = 0.6$, the amplitude of $\langle O(\theta)\rangle$ can be obtained, as shown in Fig. 3.

From Fig. 3, a black hole as an obstacle has given rise to the diffraction of the scalar wave, which further results in the observed interference pattern, which coincides with that found in the Schwarzschild AdS black hole. In addition, it shows that all peaks of the amplitude increased with the $f(R)$ parameter $\psi_0$ but decreased with the even horizon $r_h$, frequency $\omega$, and parameter $\eta$. In other words, the amplitude of the response function has the features of a space-time geometry.

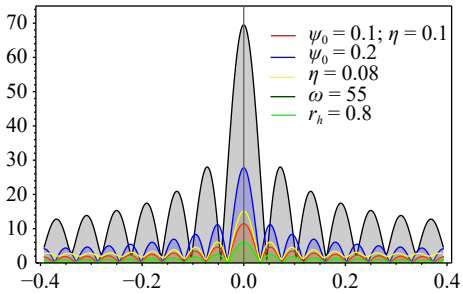


**Fig. 3** Amplitude of $|\langle O\rangle|$ around the North Pole.

## 4 Holographic rings of an AdS black hole in $f(R)$ gravity

After obtaining the total response function, we present it on a spherical screen. Based on Fig. 2(b), the lens with the focus located at $z=\pm f$ is assumed to be infinitely thin, and $f$ is assumed to be much larger than the size of the lens, i.e., $f \gg d$. When the response function is copied as a plane wave around the observed point, we obtain $\Psi_p = \langle O\rangle$. After the plane wave is converted into a wave transmitted with a lens, the wave function $\Psi_s(\boldsymbol{x})$ on the lens can be written as

$$\Psi_s(\boldsymbol{x}) = \mathrm{e}^{-\mathrm{i}\omega\frac{|\boldsymbol{x}|^2}{2f}}\Psi_p(\boldsymbol{x}), \tag{18}$$

where $\omega$ denotes frequency. When this wave reaches the screen, it is converted into

$$\Psi_{sc}(\boldsymbol{x}_s) = \int_{|\boldsymbol{x}|<d}\mathrm{d}x^2\Psi_s(\boldsymbol{x})\mathrm{e}^{-\mathrm{i}\omega L}. \tag{19}$$

With the aid of the relation $L=\sqrt{(x_s-x)^2+(y_s-y)+z_s^2}\simeq f-\frac{\boldsymbol{x}_s\cdot\boldsymbol{x}}{f}+\frac{|\boldsymbol{x}|^2}{2f}$, and further considering the Fresnel approximation, i.e., $f\gg|\boldsymbol{x}|$, one can obtain

$$\Psi_{sc}(\boldsymbol{x}_s)\propto\int_{|\boldsymbol{x}|<d}\mathrm{d}x^2\Psi_p(\boldsymbol{x})\varpi(\boldsymbol{x})\mathrm{e}^{-\frac{\mathrm{i}\omega}{f}\boldsymbol{x}\cdot\boldsymbol{x}_s}, \tag{20}$$

with

$$\varpi(\boldsymbol{x}) \equiv \begin{cases}1, & 0\le|\boldsymbol{x}|\le d\\ 0, & |\boldsymbol{x}|>d\end{cases}, \tag{21}$$

where the Taylor expansion and appropriate approximations are used to obtain Eq. (20), and $\varpi(\boldsymbol{x})$ is a window function. Therefore, images of dual black holes on the screen can be captured. The holographic Einstein rings can be obtained by choosing the appropriate values of the black hole parameters and are presented in Fig. 4 when the observed point is located at different positions.

As shown in Fig. 4, a series of concentric striped

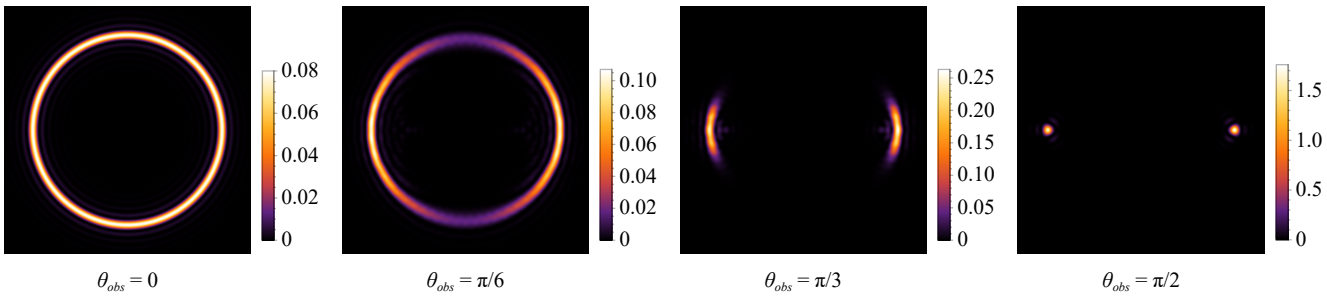


**Fig. 4** The holographic images for $\psi_0 = 0.1, \eta = 0.25, \omega = 75, r_h = 0.75, d = 0.6, \sigma = 0.05$, where the vertical line reads $y_s/f$ and horizontal axis is $x_s/f$, and their range belongs to $(-1.3, 1.3)$, which also used in later similar figures.

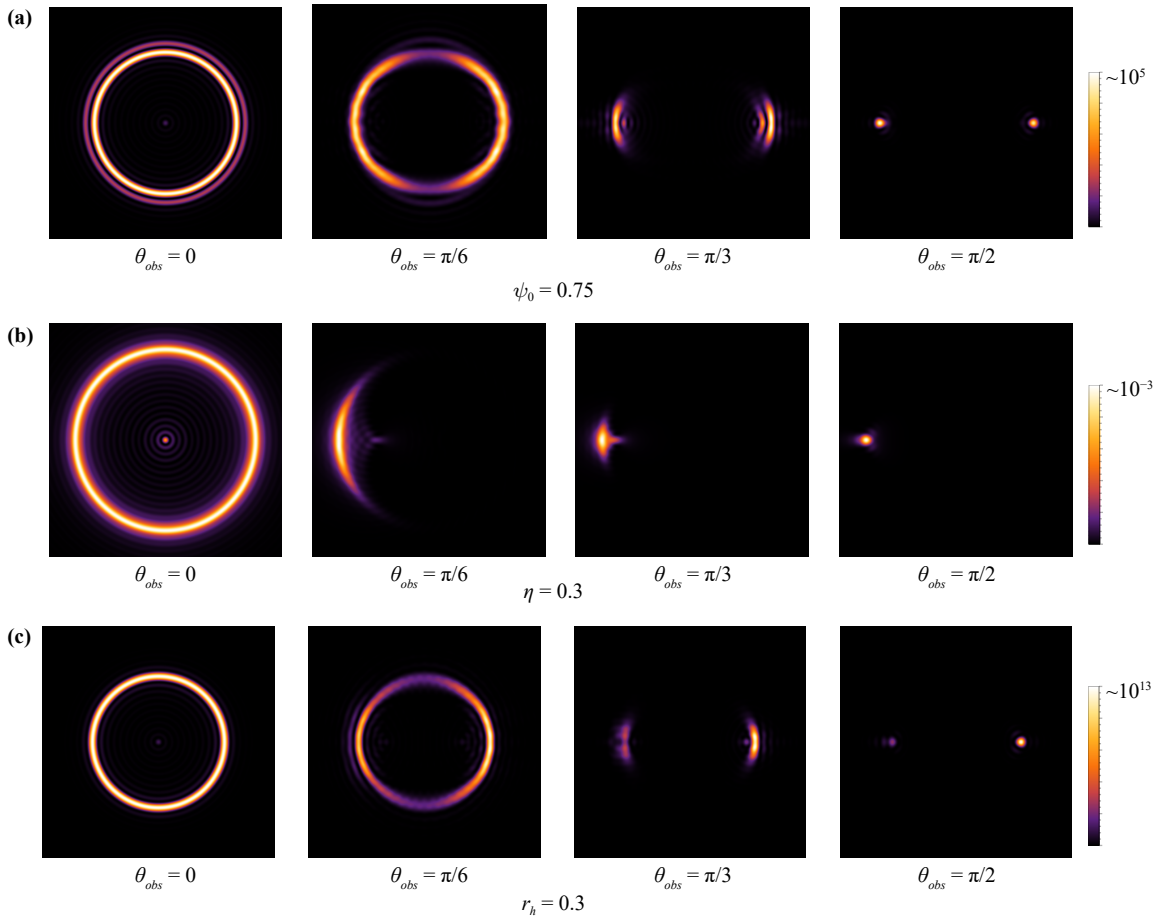


**Fig. 5** Holographic images for $d = 0.6, \sigma = 0.05, \omega = 75$.

patterns are caused by the diffraction of the scalar wave. There seems to be nothing at the center of the holographic Einstein ring. In fact, there is a light point which is so weak that we cannot see it. The choice of parameters causes this problem. This brighter light point can be seen in the following figures, i.e., the first column of Fig. 5, and is analogous to the Poisson–Arago spot. More importantly, one can see that the holographic ring of the dual black hole is closely related to the observer's position. For instance, this evolves into a luminosity-deformed ring rather than a rotationally symmetric ring. In addition, this ring is reduced to two points at $\theta_{obs} = \pi/2$, as explained by geometrical optics in later discussions. The maximum intensity of the ring increases with the increase of $\theta_{obs}$. In addition, we obtained holographic rings with different values of the chosen black hole parameters, that is, $\psi_0, \eta, r_h$, which are shown in Fig. 5.

By comparing with Fig. 4, one can see from Fig. 5 that the radius of the ring decreases with the $f(R)$ parameter $\psi_0$ but increases with the event horizon $r_h$ when the observed position $\theta_{obs} = 0$. Although the global

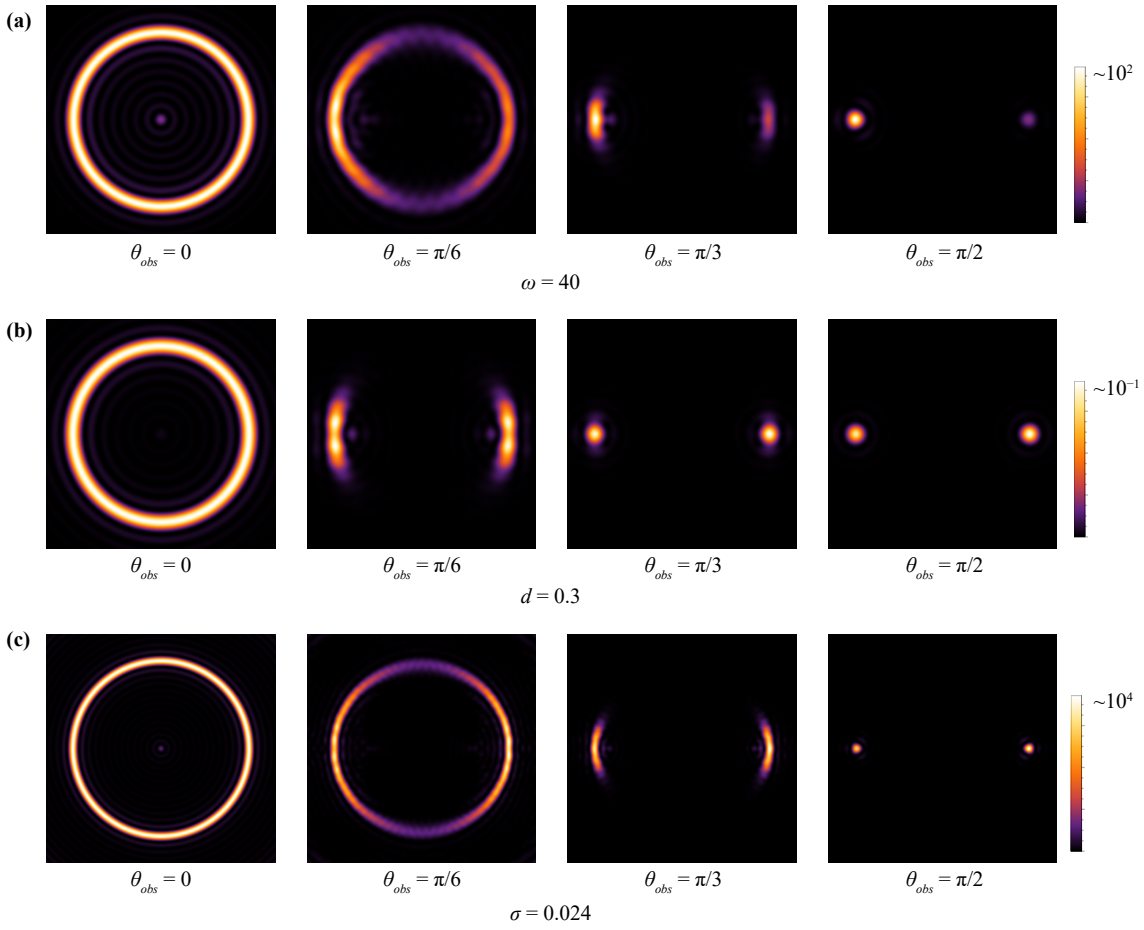


**Fig. 6** Holographic images for $\psi_0 = 0.25, \eta = 0.1, r_h = 0.75$.

monopole parameter $\eta$ has almost no effect on the radius of the ring, it increases the width of the holographic Einstein ring. Meanwhile, the concentric striped patterns caused by wave diffraction appear more evident than those observed in Fig. 4. In particular, the brighter point at the center that interfered with the concentric ring of the holographic Einstein ring became increasingly brighter as parameter $\eta$ increases. We also find that the maximum intensity of the ring increases with $\psi_0$, but decreases with $\eta$ and $r_h$. In our study, the diffraction intensity increases when the event horizon $r_h$ is larger. In this case, an increasing number of waves are superimposed at the ring's location, and the total intensity increases naturally, which implies that the intensity of the ring increases when $r_h$ decreases. At other observed positions, there are many different features for different values of black hole parameters, as shown in Fig. 4. For instance, when one increases $\psi_0$, the holographic images seem symmetric regardless of the intensity or shape for $\theta_{obs} = \pi/6$, but they evolve into two asymmetric light arcs and light spots with surrounding concentric striped patterns, as shown in Fig. 5(a). Moreover, in Fig. 5(b), where $\eta = 0.3$, the brightness of the ring on the left and right sides is no longer symmetrical for $\theta_{obs} = \pi/6$, $\pi/3$ and $\pi/2$, and the right light spot disappears. In addition, we find that different values of $r_h$ lead to different appearances of holographic rings at different positions. Based on these observations, we can conclude that the holographic images shown in Figs. 4 and 5 not only characterize the feature of space-time geometry but may also be more suitable with expectations for a given quantum system.

For different values of the optical system and source, that is, $d$, $\sigma$, and $\omega$, we present the corresponding holographic rings in Fig. 6.

Based on Fig. 6, we find that the width of the ring will be larger for a smaller value of $d$ or $\omega$, but unchanged for $\sigma$[1)]. It is worth noting that the sizes of the rings are hardly affected by these parameters. In addition, when the observer is located at $\theta_{obs} = 0$, the intensity of the concentric striped patterns increases with a decrease in $\sigma$ and $\omega$, but increases with the increase of the lens parameter $d$. At the other observed points, as the size of the lens decreases to $d = 0.3$, the

[1)] Here, to hold on the source as the Gaussian wave, we only change $\sigma$ in a small acceptable region.

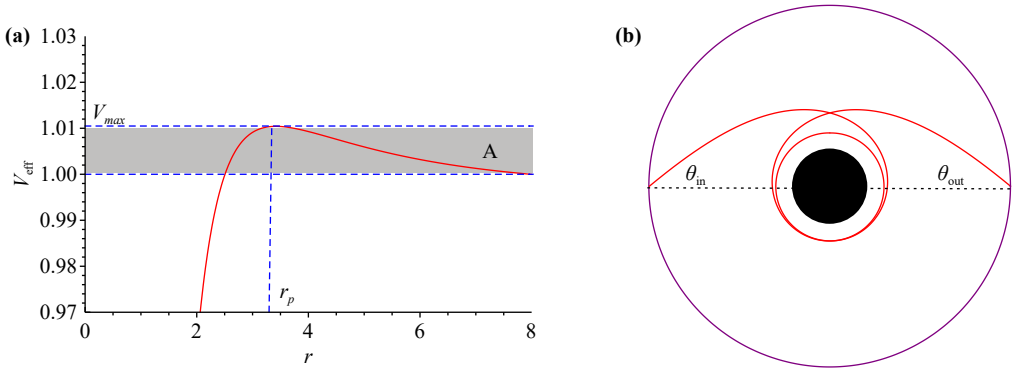


**Fig. 7** Effective potential and photon orbit.

holographic ring is quickly reduced to two points at $\theta_{obs} = \pi/3$, whereas for $d = 0.6$ it occurs at $\theta_{obs} = \pi/2$. In addition, the decrease in $\omega$ also increases the disparity in luminosity between the two light spots at position $\theta_{obs} = \pi/2$, and the right spot is evidently darker. In other words, it is found that holographic images are related to the space-time geometry of black holes and the nature of the lens and source $\mathcal{J}_O$.

However, to understand the holographic ring more clearly, we clarify the holographic Einstein ring in another way, that is, through geometrical optics. For simplicity, the orbital plane of a photon can always be fixed on the equatorial plane when the black hole is spherically symmetric. Under this condition, $\theta = \pi/2$ and $\dot{\theta} = 0$. Therefore, as we draw attention back to the coordinates $(t, r, \theta, \varphi)$, the Lagrangian $\mathcal{L}$ of a particle can be written as

$$\mathcal{L} = \frac{1}{2} g_{\mu\nu} \dot{x}^\mu \dot{x}^\nu = \frac{1}{2} \left[ -A(r)\dot{t}^2 + \frac{\dot{r}^2}{A(r)} + r^2 \dot{\varphi}^2 \right], \quad (22)$$

where $\dot{x}^\mu = \partial x^\mu / \partial \lambda$ is the 4-velocity of the light ray, and $\lambda$ is the affine parameter. Because metric $A(r)$ does not contain time $t$ or azimuthal angle $\varphi$, there are two conserved quantities:

$$E = -\frac{\partial \mathcal{L}}{\partial \dot{t}} = A(r)\dot{t}, \quad L = \frac{\partial \mathcal{L}}{\partial \dot{\varphi}} = r^2 \dot{\varphi}. \quad (23)$$

From the null geodesic $g_{\mu\nu}\dot{x}^\mu \dot{x}^\nu = 0$, we obtain

$$\dot{r}^2 + V(r) = \frac{1}{b^2}, \quad (24)$$

where $b \equiv L/E$ is the impact parameter, and $\lambda$ is redefined as $\lambda/L$ in Eq. (24). The effective potential can be expressed as follows:

$$V(r) \equiv \frac{A(r)}{r^2} = \frac{(r-r_h)\left[16\pi\eta^2 + r_h\,(3r\psi_0 - 2)\,(r_h + r - \psi_0) + 2r\,(\psi_0 - r) - 2\right]}{r^3\,(3\psi_0 r_h - 2)}. \quad (25)$$

The effective potentials are shown in Fig. 7(a) by taking $M = 1, \psi_0 = 0.1, \eta = 0.1, \ell = 10$ as an example. At the photon-sphere position, $V(r)$ should satisfy $V = 1/b^2$ and $V' = 0$ by considering the conditions $\dot{r} = 0$ and $\ddot{r} = 0$. Using this assumption, it is easy to determine that the location of the photon sphere $r_p$ corresponds to the maximum value $V_{max} = V(r)\,|_{r=r_p}$, and the impact parameter is $b_p = 1/\sqrt{V_{max}}$ in this case. Generally, when a photon with different impact parameters passes through the vicinity of a black hole, it exhibits different motion behaviors. As the observer should capture the photon at the AdS boundary from the light source, we mainly focus on the case in which the dual black hole to the AdS boundary reflects the photon. This case corresponds to Region A in Fig. 7(a), where $b > b_p$. Because $\lim_{r\to\infty} V(r) = 1$, the range of region A is $(1, V_{max})$; thus, the impact parameter should satisfy $1 < \frac{1}{b^2} < V_{max}$. If a photon passes through a position very close to the photon sphere, it may surround the black hole several times before reaching the observer. The closer the photon sphere is to the photon, the more photons circle the black hole. This implies that an infinite accumulation of photons occurs at this position. Figure 7(b) shows the schematic diagram of light rays when they circle the black hole two times, where two endpoints of the photon orbit and the center of the black hole are in a straight line. In this case, the incident angle $\theta_{in}$ between the photon orbit and the radial direction is equal to the emitted angle $\theta_{out}$, which can be expressed as

$$\cos\theta_{in} = g_{ij} \frac{u^i n^j}{|u||n|}\bigg|_{r\to\infty}, \quad (26)$$

where $u^i$ is the spatial component of the 4-velocity, and $n^j$ is the normal vector. With the help of Eqs. (23) and (24), we obtain

$$\sin\theta_{in} = \frac{L}{E}. \quad (27)$$

Therefore, the infinitely accumulated position of a photon can be expressed as $\sin\theta_{in}$, which corresponds to location $r_p$ where $b_p = \frac{1}{\sqrt{V_{max}}}$. Owing to the axisymmetry,

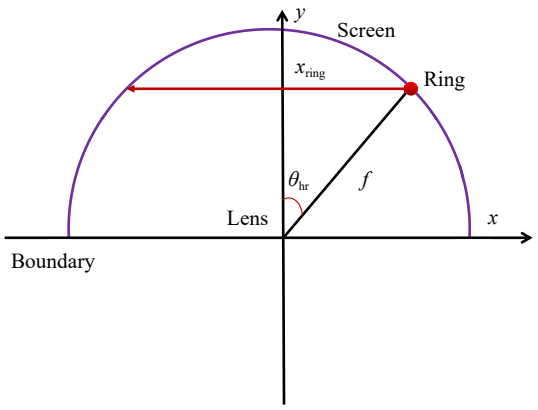


**Fig. 8** Angle $\theta_{hr}$ in Eq. (28).

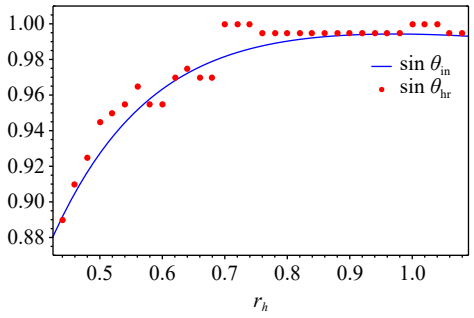


**Fig. 9** Radius of the photon sphere and holographic Einstein ring.

the observer can see a bright ring, and its radius is closely related to $r_p$ in geometrical optics.

To characterize the radius of the holographic ring, as shown in Fig. 4, we can make the following definition:

$$\sin\theta_{\rm hr} = \frac{x_{\rm ring}}{f}, \tag{28}$$

where at position $x_s = x_{\rm ring}$, $|\Psi_{sc}|^2$ has a maximum value, and only the $x_s$ axis is considered for the $(x_s, y_s)$ plane. A diagram of angle $\theta_{\rm hr}$ is shown in Fig. 8.

The superposed spherical harmonics form a wave packet, which is exactly the null geodesic in wave optics. Therefore, when the spherical harmonics $Y_{\ell 0} \sim {\rm e}^{{\rm i}\ell\theta}$ in Eq. (20) [74], the image peak occurs at

$$\frac{x_{\rm ring}}{f} \simeq \frac{\ell}{\omega}. \tag{29}$$

Because $\ell$ and $\omega$ in wave optics coincide with the angular momentum and energy in geometrical optics, we have $\frac{L}{E} = \frac{\ell}{\omega}$. This implies that $\sin\theta_{\rm in} \simeq \sin\theta_{\rm hr}$, which implies that the size of the holographic ring is consistent with that of the photon ring obtained using geometrical optics. Therefore, the infinite accumulation of photons in the photon sphere gives rise to the brightest ring, which corresponds to the maximum value of $|\Psi_{sc}|^2$ from the viewpoint of wave optics. In addition, because $\theta_{obs} = \pi/2$ in Fig. 4, the two light points correspond to the clockwise light rays and anticlockwise one around the black hole, respectively. We numerically extracted the holographic ring data to check Eq. (29) and plotted the photon sphere.

From Fig. 9, it is evident that the red points are always located at the region in the neighborhood of the blue line, which means the radius of the holographic Einstein ring coincides with that of the photon sphere. Therefore, one can see that the holographic Einstein images obtained using wave optics are credible because they are in line with those obtained using geometric optics.

## 5 Discussion and conclusions

In this study, by considering a scalar wave generated by the source $\mathcal{J}_O$ on the AdS boundary, we employ the corresponding response function to carefully investigate the holographic images of an AdS black hole using $f(R)$ gravity theory from wave optics. Specifically, we use the Klein–Gordon equation to study the dynamics of a massless scalar field and obtain the response function based on the AdS/CFT dictionary. By introducing an optical system, holographic images of the dual black hole on the screen are captured, and we clarify them using geometrical optics. In addition, the effects of black holes and lens parameters on the holographic images are discussed throughout the paper.

The results reveal that the interference patterns that originate from the diffraction of the scalar wave are always observed for the total response function $\langle O\rangle$. Its amplitude increases with the $f(R)$ parameter $\psi_0$ but decreases with the global monopole parameter $\eta$, frequency $\omega$, and horizon $r_h$. In other words, modified gravity may strengthen the interference pattern, whereas the global monopole weakens it. On the screen, when the observer is located at $\theta_{obs} = 0$, we can observe a perfect Einstein ring and a Poisson-like spot surrounded by a series of concentric striped patterns. At other positions, that is, $\theta_{obs} = \pi/6$ and $\pi/3$, the ring breaks and forms a luminosity-deformed ring. In particular, at $\theta_{obs} = \pi/2$, the ring finally evolves into two light spots. For different values of black hole and lens parameters, some noteworthy features are shown in Figs. 5 and 6. For instance, it turns out that the $f(R)$ parameter $\psi_0$ decreases the radius of the holographic Einstein ring but hardly influences its width. In addition, an increase in the global monopole parameter $\eta$ seems to give rise to more apparent concentric striped patterns, even if the radius of the ring remains unchanged. Parameter $\psi_0$ increases the intensity of the ring, whereas $\eta$ decreases it. We also find that the width of the ring is smaller for smaller values of the horizon radius of the black hole $r_h$, but the intensity increases. For the lens and source parameters, the results reveal that the radius of the ring does not always

change with $d$ and $\omega$; however, the width increases with a decrease in $d$ and $\omega$. In addition, the intensity decreases with $\omega$ but hardly changes with $d$. Parameter $\sigma$ only influences the intensity of the Einstein ring, which has no effect on the radius or width. For the values of the black hole and lens parameters, the observed rings at different positions also differ. When $\eta = 0.3$ in Fig. 5, one can see that the ring is finally reduced to one light point rather than two. As the lens size decreases, the holographic ring evolves into two light spots more quickly as the position $\theta$ increases, that is, $\theta_{obs} = \pi/3$ in the second row of Fig. 6. For smaller $\omega$ and $d$, the holographic rings are blurry when compared to those of the larger values. For the effect of the $f(R)$ parameter $\psi_0$, an increase in the $f(R)$ parameter $\psi_0$ generally increases the space-time curvature. This further indicates that the gravity to which the photon is subjected also increases. As a result, the photon ring (or holographic Einstein ring) will become increasingly smaller, but the width remains unchanged. Moreover, it is evident that the stronger the gravity, the larger the intensity of the ring, as well as the maximum intensity. We can see that the effect of the $f(R)$ gravity is so important that it cannot be neglected while studying a holographic Einstein ring. In other words, the holographic Einstein ring of an AdS black hole is closely related to the black hole, lens, and source parameters. Finally, we conclude that the holographic rings of an AdS black hole in modified gravities are more suitable and helpful for testing the existence of a gravity dual for a given material because they are more abundant in those gravities.

In addition, the study of holographic rings using other gravity theories remains a topic for the near future. In addition, holographic rings can be extended to observe black holes in superconductors [75]. Considering this method for p- and d-wave holographic superconductor models is also a worthwhile future research pursuit.

**Declarations** The authors declare that they have no competing interests and there are no conflicts.

**Acknowledgements** This work was supported by the National Natural Science Foundation of China (Grant No. 11903025), the Starting Fund of China West Normal University (Grant No. 18Q062), the Natural Science Foundation of Sichuan Province (Grant No. 2022NSFSC1833), the Sichuan Science and Technology Program (No. 2023ZYD0023), the Sichuan Youth Science and Technology Innovation Research Team (Grant No. 21CXTD0038), the Chongqing Science and Technology Bureau (Grant No. cstc2022ycjh-bgzxm0161), and the Basic Research Project of Science and Technology Committee of Chongqing (Grant No. CSTB2023NSCQ-MSX0324).

## References

1. G. 't Hooft, Dimensional reduction in quantum gravity, arXiv: gr-qc/9310026 (1993)
2. L. Susskind, The world as a hologram, *J. Math. Phys.* 36(11), 6377 (1995)
3. J. M. Maldacena, The large $N$ limit of superconformal field theories and supergravity, *Adv. Theor. Math. Phys.* 2(2), 231 (1998)
4. E. Witten, Anti-de Sitter space and holography, *Adv. Theor. Math. Phys.* 2(2), 253 (1998)
5. S. S. Gubser, I. R. Klebanov, and A. M. Polyakov, Gauge theory correlators from noncritical string theory, *Phys. Lett. B* 428(1–2), 105 (1998)
6. J. Erlich, E. Katz, D. T. Son, and M. A. Stephanov, QCD and a holographic model of hadrons, *Phys. Rev. Lett.* 95(26), 261602 (2005)
7. S. A. Hartnoll, C. P. Herzog, and G. T. Horowitz, Building a holographic superconductor, *Phys. Rev. Lett.* 101(3), 031601 (2008)
8. T. Damour, in: Proceedings of the Second Marcel Grossmann Meeting on General Relativity, edited by R. Ruffini, North Holland, Amsterdam, p. 587, 1982
9. G. Policastro, D. T. Son, and A. O. Starinets, From AdS/CFT correspondence to hydrodynamics, *J. High Energy Phys.* 09, 043 (2002)
10. S. Bhattacharyya, V. E. Hubeny, S. Minwalla, and M. Rangamani, Nonlinear fluid dynamics from gravity, *J. High Energy Phys.* 02, 045 (2008)
11. S. Kachru, X. Liu, and M. Mulligan, Gravity duals of Lifshitz-like fixed points, *Phys. Rev. D* 78(10), 106005 (2008)
12. D. T. Son, Toward an AdS/cold atoms correspondence: A geometric realization of the Schrodinger symmetry, *Phys. Rev. D* 78(4), 046003 (2008)
13. K. Balasubramanian and J. McGreevy, Gravity duals for nonrelativistic conformal field theories, *Phys. Rev. Lett.* 101(6), 061601 (2008)
14. C. Charmousis, B. Goutéraux, B. Soo Kim, E. Kiritsis, and R. Meyer, Effective holographic theories for low-temperature condensed matter systems, *J. High Energy Phys.* 2010(11), 151 (2010)
15. B. Gouteraux and E. Kiritsis, Generalized holographic quantum criticality at finite density, *J. High Energy Phys.* 1112, 036 (2011)
16. S. Ryu and T. Takayanagi, Holographic derivation of entanglement entropy from the anti-de Sitter space/conformal field theory correspondence, *Phys. Rev. Lett.* 96(18), 181602 (2006)
17. S. Ryu and T. Takayanagi, Aspects of holographic entanglement entropy, *J. High Energy Phys.* 08, 045 (2006)
18. E. Tonni, Holographic entanglement entropy: Near horizon geometry and disconnected regions, *J. High Energy Phys.* 05, 004 (2011)
19. D. Stanford and L. Susskind, Complexity and shock wave geometries, *Phys. Rev. D* 90(12), 126007 (2014)
20. M. Li, A model of holographic dark energy, *Phys. Lett. B* 603(1–2), 1 (2004)
21. R. G. Cai, A dark energy model characterized by the age of the universe, *Phys. Lett. B* 657(4–5), 228 (2007)
22. C. Gao, F. Wu, X. Chen, and Y. G. Shen, A holographic dark energy model from Ricci scalar curvature, *Phys. Rev. D* 79(4), 043511 (2009)
23. A. Strominger, The dS/CFT correspondence, *J. High*

*Energy Phys.* 10, 034 (2001)
24. I. Bredberg, C. Keeler, V. Lysov, and A. Strominger, Lectures on the Kerr/CFT correspondence, *Nucl. Phys. B Proc. Suppl.* 216(1), 194 (2011)
25. Q. G. Huang and M. Li, The holographic dark energy in a non-flat universe, *J. Cosmol. Astropart. Phys.* 08, 013 (2004)
26. X. Zhang and F. Q. Wu, Constraints on holographic dark energy from Type Ia supernova observations, *Phys. Rev. D* 72(4), 043524 (2005)
27. B. Wang, Y. Gong, and E. Abdalla, Thermodynamics of an accelerated expanding universe, *Phys. Rev. D* 74(8), 083520 (2006)
28. J. Jing and S. Chen, Holographic superconductors in the Born–Infeld electrodynamics, *Phys. Lett. B* 686(1), 68 (2010)
29. J. P. Wu, Y. Cao, X. M. Kuang, and W. J. Li, The 3+1 holographic superconductor with Weyl corrections, *Phys. Lett. B* 697(2), 153 (2011)
30. Y. Ling, C. Niu, J. Wu, Z. Xian, and H. B. Zhang, Metal–insulator transition by holographic charge density waves, *Phys. Rev. Lett.* 113(9), 091602 (2014)
31. R. G. Cai, L. Li, L. F. Li, and R. Q. Yang, Introduction to holographic superconductor models, *Sci. China Phys. Mech. Astron.* 58(6), 060401 (2015)
32. X. X. Zeng, H. Zhang, and L. F. Li, Phase transition of holographic entanglement entropy in massive gravity, *Phys. Lett. B* 756, 170 (2016)
33. Y. Kusuki, J. Kudler-Flam, and S. Ryu, Derivation of holographic negativity in $AdS_3/CFT_2$, *Phys. Rev. Lett.* 123(13), 131603 (2019)
34. C. Akers, N. Engelhardt, and D. Harlow, Simple holographic models of black hole evaporation, *J. High Energy Phys.* 08, 032 (2020)
35. A. Bhattacharya, A. Bhattacharyya, P. Nandy, and A. K. Patra, Islands and complexity of eternal black hole and radiation subsystems for a doubly holographic model, *J. High Energy Phys.* 2021(5), 135 (2021)
36. S. Nojiri, S. D. Odintsov, and V. Faraoni, From nonextensive statistics and black hole entropy to the holographic dark universe, *Phys. Rev. D* 105(4), 044042 (2022)
37. P. Karndumri, Holographic RG flows and symplectic deformations of $N$=4 gauged supergravity, *Phys. Rev. D* 105(8), 086009 (2022)
38. Y. K. Yan, S. Lan, Y. Tian, P. Yang, S. Yao, and H. Zhang, Holographic dissipation prefers the Landau over the Keldysh form, *Phys. Rev. D* 107, L121901 (2023)
39. S. Lan, X. Li, J. Mo, Y. Tian, Y. K. Yan, P. Yang, and H. Zhang, Splitting of doubly quantized vortices in holographic superfluid of finite temperature, *J. High Energy Phys.* 2023(5), 223 (2023)
40. S. Yao, Y. Tian, P. Yang, and H. Zhang, Baby skyrmion in two-component holographic superfluids, *J. High Energy Phys.* 08, 055 (2023)
41. B. P. Abbott, R. Abbott, T. D. Abbott, M. R. Abernathy, F. Acernese, et al., Observation of gravitational waves from a binary black hole merger, *Phys. Rev. Lett.* 116(6), 061102 (2016)
42. K. Akiyama, A. Alberdi, W. Alef, K. Asada, R. Azulay, et al. [Event Horizon Telescope Collaboration], First M87 event horizon telescope results. I. The shadow of the supermassive black hole, *Astrophys. J. Lett.* 875(1), L1 (2019)
43. K. Akiyama, et al. [Event Horizon Telescope Collaboration], First sagittarius $A^*$ event horizon telescope results. I. The shadow of the supermassive black hole in the center of the Milky Way, *Astrophys. J. Lett.* 930(2), L12 (2022)
44. S. W. Wei, P. Cheng, Y. Zhong, and X. N. Zhou, Shadow of noncommutative geometry inspired black hole, *J. Cosmol. Astropart. Phys.* 08, 004 (2015)
45. M. Guo, N. A. Obers, and H. Yan, Observational signatures of near-extremal Kerr-like black holes in a modified gravity theory at the Event Horizon Telescope, *Phys. Rev. D* 98(8), 084063 (2018)
46. S. W. Wei, Y. C. Zou, Y. X. Liu, and R. B. Mann, Curvature radius and Kerr black hole shadow, *J. Cosmol. Astropart. Phys.* 08, 030 (2019)
47. H. M. Wang, Y. M. Xu, and S. W. Wei, Shadows of Kerr-like black holes in a modified gravity theory, *J. Cosmol. Astropart. Phys.* 03, 046 (2019)
48. M. Guo and P. C. Li, Innermost stable circular orbit and shadow of the 4D Einstein–Gauss–Bonnet black hole, *Eur. Phys. J. C* 80(6), 588 (2020)
49. F. Long, J. Wang, S. Chen, and J. Jing, Shadow of a rotating squashed Kaluza–Klein black hole, *J. High Energy Phys.* 2019(10), 269 (2019)
50. Z. Hu, Z. Zhong, P. C. Li, M. Guo, and B. Chen, QED effect on a black hole shadow, *Phys. Rev. D* 103(4), 044057 (2021)
51. Y. Chen, P. Wang, H. Wu, and H. Yang, Observational appearance of a freely-falling star in an asymmetric thin-shell wormhole, *Eur. Phys. J. C* 83(5), 361 (2023)
52. Y. Hou, Z. Zhang, H. Yan, M. Guo, and B. Chen, Image of a Kerr–Melvin black hole with a thin accretion disk, *Phys. Rev. D* 106(6), 064058 (2022)
53. Q. Gan, P. Wang, H. Wu, and H. Yang, Photon spheres and spherical accretion image of a hairy black hole, *Phys. Rev. D* 104(2), 024003 (2021)
54. S. E. Gralla, D. E. Holz, and R. M. Wald, Black hole shadows, photon rings, and lensing rings, *Phys. Rev. D* 100(2), 024018 (2019)
55. X. X. Zeng and H. Q. Zhang, Influence of quintessence dark energy on the shadow of black hole, *Eur. Phys. J. C* 80(11), 1058 (2020)
56. X. X. Zeng, H. Zhang, and H. Q. Zhang, Shadows and photon spheres with spherical accretions in the four-dimensional Gauss–Bonnet black hole, *Eur. Phys. J. C* 80(9), 872 (2020)
57. G. P. Li and K. J. He, Shadows and rings of the Kehagias–Sfetsos black hole surrounded by thin disk accretion, *J. Cosmol. Astropart. Phys.* 06, 037 (2021)
58. G. P. Li and K. J. He, Observational appearances of a $f(R)$ global monopole black hole illuminated by various accretions, *Eur. Phys. J. C* 81(11), 1018 (2021)
59. K. J. He, S. C. Tan, and G. P. Li, Influence of torsion charge on shadow and observation signature of black hole surrounded by various profiles of accretions, *Eur. Phys. J. C* 82(1), 81 (2022)
60. K. J. He, S. Guo, S. C. Tan, and G. P. Li, Shadow

images and observed luminosity of the Bardeen black hole surrounded by different accretions, *Chin. Phys. C* 46, 085106 (2021)
61. X. X. Zeng, K. J. He, and G. P. Li, Effects of dark matter on shadows and rings of brane-world black holes illuminated by various accretions, *Sci. China Phys. Mech. Astron.* 65(9), 290411 (2022)
62. J. Peng, M. Guo, and X. H. Feng, Influence of quantum correction on the black hole shadows, photon rings and lensing rings, *Chin. Phys. C* 45, 085103 (2021)
63. X. X. Zeng, G. P. Li, and K. J. He, The shadows and observational appearance of a noncommutative black hole surrounded by various profiles of accretions, *Nucl. Phys. B* 974, 115639 (2022)
64. H. M. Wang, Z. C. Lin, and S. W. Wei, Optical appearance of Einstein–Æther black hole surrounded by thin disk, *Nucl. Phys. B* 985, 116026 (2022)
65. A. Lapi, M. Negrello, J. González-Nuevo, Z. Y. Cai, G. De Zotti, and L. Danese, Effective models for statistical studies of galaxy-scale gravitational lensing, *Astrophys. J.* 755(1), 46 (2012)
66. D. J. Lagattuta, S. Vegetti, C. D. Fassnacht, M. W. Auger, L. V. E. Koopmans, and J. P. McKean, SHARP-I. A high-resolution multi-band view of the infra-red Einstein ring of JVAS B1938+666, *Mon. Not. R. Astron. Soc.* 424(4), 2800 (2012)
67. S. Sahu, M. Patil, D. Narasimha, and P. S. Joshi, Can strong gravitational lensing distinguish naked singularities from black holes, *Phys. Rev. D* 86(6), 063010 (2012)
68. P. L. Kelly, S. A. Rodney, T. Treu, R. J. Foley, G. Brammer, et al., Multiple images of a highly magnified supernova formed by an early-type cluster galaxy lens, *Science* 347(6226), 1123 (2015)
69. A. Goobar, R. Amanullah, S. R. Kulkarni, P. E. Nugent, J. Johansson, et al., iPTF16geu: A multiply imaged, gravitationally lensed type Ia supernova, *Science* 356(6335), 291 (2017)
70. R. Li, C. S. Frenk, S. Cole, Q. Wang, and L. Gao, Projection effects in the strong lensing study of subhaloes, *Mon. Not. R. Astron. Soc.* 468(2), 1426 (2017)
71. R. B. Metcalf, M. Meneghetti, C. Avestruz, F. Bellagamba, C. R. Bom, et al., The strong gravitational lens finding challenge, *Astron. Astrophys.* 625, A119 (2019)
72. F. Tamburini, B. Thidé, and M. Della Valle, Measurement of the spin of the M87 black hole from its observed twisted light, *Mon. Not. R. Astron. Soc.* 492(1), L22 (2020)
73. K. Hashimoto, S. Kinoshita, and K. Murata, Einstein rings in holography, *Phys. Rev. Lett.* 123(3), 031602 (2019)
74. K. Hashimoto, S. Kinoshita, and K. Murata, Imaging black holes through the AdS/CFT correspondence, *Phys. Rev. D* 101(6), 066018 (2020)
75. Y. Kaku, K. Murata, and J. Tsujimura, Observing black holes through superconductors, *J. High Energy Phys.* 2021(9), 138 (2021)
76. Y. Liu, Q. Chen, X. X. Zeng, H. Zhang, and W. Zhang, Holographic Einstein ring of a charged AdS black hole, *J. High Energy Phys.* 2022(10), 189 (2022)
77. X. X. Zeng, K. J. He, J. Pu, G. P. Li, and Q. Q. Jiang, Holographic Einstein rings of a Gauss–Bonnet AdS black hole, *Eur. Phys. J. C* 83(10), 897 (2023)
78. X. X. Zeng, L. F. Li, and P. Xu, Holographic Einstein rings of a black hole with a global monopole, arXiv: 2307.01973 (2023)
79. X. Y. Hu, M. I. Aslam, R. Saleem, and X. X. Zeng, Holographic Einstein rings of an AdS black hole in massive gravity, *J. Cosmol. Astropart. Phys.* 11, 013 (2023), arXiv: 2308.05132v2
80. X. Y. Hu, X. X. Zeng, L. F. Li, and P. Xu, Holographic Einstein rings of non-commutative black holes, arXiv: 2309.07404 (2023)
81. X. X. Zeng, M. Israr Aslam, R. Saleem, and X. Y. Hu, Holographic Einstein rings of black holes in scalar-tensor-vector gravity, arXiv: 2311.04680 (2023)
82. C. M. Will, The confrontation between general relativity and experiment, *Living Rev. Relativ.* 17(1), 4 (2014)
83. A. De Felice and S. Tsujikawa, Excluding static and spherically symmetric black holes in Einsteinian cubic gravity with unsuppressed higher-order curvature terms, *Phys. Lett. B* 843, 138047 (2023)
84. H. A. Buchdahl, Non-linear Lagrangians and cosmological theory, *Mon. Not. R. Astron. Soc.* 150(1), 1 (1970)
85. S. Nojiri and S. D. Odintsov, Modified gravity with negative and positive powers of curvature: Unification of inflation and cosmic acceleration, *Phys. Rev. D* 68(12), 123512 (2003)
86. S. M. Carroll, V. Duvvuri, M. Trodden, and M. S. Turner, Is cosmic speed-up due to new gravitational physics, *Phys. Rev. D* 70(4), 043528 (2004)
87. S. Fay, R. Tavakol, and S. Tsujikawa, $f(R)$ gravity theories in Palatini formalism: Cosmological dynamics and observational constraints? *Phys. Rev. D* 75(6), 063509 (2007)
88. T. R. P. Caramês, E. R. Bezerra De Mello, and M. E. X. Guimarães, Gravitational field of a global monopole in a modified gravity, *Int. J. Mod. Phys. Conf. Ser.* 3, 446 (2011)
89. J. Man and H. Cheng, Thermodynamic quantities of a black hole with an $f(R)$ global monopole, *Phys. Rev. D* 87(4), 044002 (2013)
90. J. P. Morais Graça, I. P. Lobo, and I. G. Salako, Cloud of strings in $f(R)$ gravity, *Chin. Phys. C* 42(6), 063105 (2018)
91. J. R. Nascimento, G. J. Olmo, P. J. Porfirio, A. Yu. Petrov, and A. R. Soares, Global monopole in palatini $f(R)$ gravity, *Phys. Rev. D* 99(6), 064053 (2019)
92. J. Man and H. Cheng, Analytical discussion on strong gravitational lensing for a massive source with a $f(R)$ global monopole, *Phys. Rev. D* 92(2), 024004 (2015)
93. F. B. Lustosa, M. E. X. Guimarães, C. N. Ferreira, J. L. Neto, and J. A. Helayel-Neto, On the thermodynamical black hole stability in the space-time of a global monopole in $f(R)$ gravity, *J. High Energy Phys.* 5, 587 (2019)
94. I. S. Matos, M. O. Calvão, and I. Waga, Gravitational wave propagation in $f(R)$ models: New parametrizations and observational constraints, *Phys. Rev. D* 103(10), 104059 (2021)

95. T. Karakasis, E. Papantonopoulos, Z. Y. Tang, and B. Wang, Black holes of (2+1)-dimensional $f(R)$ gravity coupled to a scalar field, *Phys. Rev. D* 103(6), 064063 (2021)
96. S. Guo, Y. Han, and G. P. Li, Joule–Thomson expansion of a specific black hole in $f(R)$ gravity coupled with Yang–Mills field, *Class. Quantum Gravity* 37(8), 085016 (2020)
97. K. J. He, G. P. Li, and X. Y. Hu, Violations of the weak cosmic censorship conjecture in the higher dimensional $f(R)$ black holes with pressure, *Eur. Phys. J. C* 80(3), 209 (2020)
98. T. P. Sotiriou and V. Faraoni, $f(R)$ theories of gravity, *Rev. Mod. Phys.* 82(1), 451 (2010)
99. A. De Felice and S. Tsujikawa, $f(R)$ theories, *Living Rev. Relativ.* 13(1), 3 (2010)
100. T. R. P. Caramês, J. C. Fabris, E. R. Bezerra de Mello, and H. Belich, $f(R)$ global monopole revisited, *Eur. Phys. J. C* 77(7), 496 (2017)
101. H. S. Vieira, On the Schwarzschild–anti-de Sitter black hole with an $f(R)$ global monopole, *Eur. Phys. J. C* 81(12), 1143 (2021)